ROYAL SOCIETY OF CHEMISTRY

PAPER

Check for updates

Unlimited recyclable wearable sensors based on a homogeneous ionic liquid and polyvinyl alcohol network†

Yuhao Huang, [ID] Yuqi Wang, Xinyi Guan, Bowen Shi, Xi Wang, Xiaogang Chen, Anura Fernando and Xuqing Liu [ID] *

Smart wearable electronics are now of great significance in the fields of biomedical applications and environmental sensors. The development of new devices will be a continuing pivotal hotspot for human beings in future. However, contamination caused by large quantities of traditional electronic waste has already done serious damage to the reputation, especially the unignorable and irreversible environmental pollution caused by the leakage of heavy metal ions and plastic microparticles. To address the issues mentioned above, we design recyclable, flexible and stretchable homogeneous wearable sensors, which are hydrogen bonding crosslinked polyvinyl alcohol (PVA) conductive films, *via* applying ion-conductive 1-hexyl-3-methylimidazolium bromide ($[HMIM]^+Br^-$) ionic liquids, into a PVA polymer network by the freeze-thawing method. The application of $[HMIM]^+Br^-$ (Br-IL) can guarantee stable conductivity with no effect on the recyclability of the whole device. What's more, Br-IL also endows the PVA film with tuneable properties, such as enhancing the flexibility and stretchability of films which is a challenge for polymer-based electronics. Not only that, Br-IL also creates a bi-continuous ion conductive phase structure in the polymer network, which could be called a "swimming lane effect". Experiments successfully prove that the PVA/Br-IL ion-conductive films can be used for strain/temperature/humidity sensing applications with perfect recyclability and reusability.

Sustainability spotlight

According to the UN's SDG Report 2022, about 80% of e-waste has been either burnt or disposed of in landfills. However, the majority of these electronic devices consist of plastics, heavy metals, and harmful substances, and such disposal methods will contaminate the atmosphere, soil, and water, especially since, according to reports, over 17 million metric tonnes of plastic have infiltrated the oceans. To ensure responsible consumption and production, we present a novel sensor based on theoretically unlimited recyclable polyvinyl alcohol and a green solution: an ionic liquid. This device composed completely of organic material could be recycled by simple dissolution and then reproduced as a sustainable device.

1 Introduction

With the rapid development of 5G mobile networks and the internet of things (IoT), the wearable device market has now undergone exponential growth.[1–5] Recently, papers have reported about newly developed wearable devices based on various kinds of conductive polymer or inorganic particles.[6] In these devices both conductive polymers and nanoparticles, such as silver,[7] copper,[8] 2D carbon materials,[9,10] and carbon black,[11] have already offered attractive advantages. However, notwithstanding the high performance of conductive filling materials, large quantities of both consumer and industry electronics have been abandoned to become e-waste without recycling.[12–14] Due to a lack of systematic research, the inevitable loss of non-renewable metal resources and plastic microparticles during use, production and recycling processes becomes a significant issue for the development of wearable devices, not to mention that the high cost of production for conductive polymers is already an unsolved problem at the initial feedstock production stage.

In this context, for further developments in wearable devices without aggravating environmental contamination issues and high production costs, the concept of transient technology has been developed in recent years.[15] Transient technology is an emergent technology that requires devices to "disappear" into a natural or common environment without traceable remains. This technology concept has already been successfully used to design biomedical applications and environmental sensors.[16,17] In these devices, the components used based on transient

Department of Materials, University of Manchester, Manchester M13 9PL, UK. E-mail: Xuqing.liu@manchester.ac.uk

technology can maintain their complete characteristics and operational functions with reliable performance under normal use conditions. After being recycled, these devices will have a controlled end to their life, for example by dismantling their structure and making them untraceable.

Based on this new concept, a recyclable polymer-based multifunctional sensor infiltrated with an ionic liquid (IL) is reported in this work. Polyvinyl alcohol is an often-tested synthetic polymer with well-known biocompatibility, solubility and easy processing characteristics.[18–20] However, the pure PVA films could not always keep their strong mechanical properties and will be even worse if solid conductive materials were introduced, which would lead to phase separation of the solid particles under prolonged mechanical stress and ultimately to a reduction in performance. To overcome the stated problems, ionic liquids are added into the PVA polymer network which is proved to be a practical solution to prepare homogeneous biopolymer blends because of the non-volatility, recyclability, and ion-conductive properties of ionic liquids.[21–23] Numerous experimental studies have shown that, when combined with different polymers, IL/polymer composites could provide a stable, versatile and often flexible sensing platform.[24] Furthermore, based on a wide variety of IL functional characteristics, polymer/IL composites are allowed to be tuned for responses to multiple external environmental stimuli, such as heat and humidity.[25]

In the present work, this study reports on the development of a multi-response film sensor based on 1-hexyl-3-methylimidazolium bromide (Br-IL) and polyvinyl alcohol (PVA). Both materials show environmental safety and biodegradability, and so do the developed ion-conductive films. The PVA/Br-IL films' morphological, physico-chemical, thermal, mechanical and electrochemical properties were studied, together with their performance as a multi-sensing platform.

2 Results and discussion

2.1 Synthesis and characterization of the ion-conductive PVA/Br-IL film/fibre

The synthesis route and design strategy of the PVA/Br-IL film are shown in Fig. 1. First of all, polyvinyl alcohol was selected as the basic polymer network for the design of a multi-functional

sensor due to its good mechanical compliance, biological characteristics and degradability properties. Secondly, $[HMIM]^+Br^-$ was synthesised and pre-dissolved into deionized water, which aims to endow the polymer film with conductivity without affecting degradability. Then, $[HMIM]^+Br^-$ is uniformly entangled with the PVA chain in the solution to form a homogeneous mixture. Finally, the PVA/Br-IL solution is dried to form a thin and transparent film in a round Petri dish.

To explore the role of IL in the enhancement of PVA polymer networks, the morphology and microstructure of the as-obtained films were characterized using a scanning electron microscope (SEM), as shown in Fig. 2A(I)–(III). It is clearly observed that the pure PVA film shows a neat and smooth surface, while the PVA/Br-IL film consists of highly unidirectional entangled micro-fibrils, which indicates that the PVA film shows a higher crystallinity than the PVA/Br-IL film, as shown in Fig. 2B. All these fibrils at the macro level are manifestations of hydrogen-bonded PVA and $[HMIM]^+Br^-$ chains at the micro level, and this indicates that $[HMIM]^+Br^-$ will form a unidirectional network and entangle with the main polymer network to fabricate a homogeneous structure which is highly ordered with the benefit of zwitterions. Moreover, Fig. 2A(IV) and S1† show the size of a highly fine PVA fibre with $[HMIM]^+Br^-$ modified down to hundreds of nanometres. It also can be found that the same aligned polymer chain is on the surface. This is because the fibre is made from polymer bulk and the fibre shape is the result of stretching when the orientation of PVA chains in the polymer is redirected. In addition, energy-dispersive X-ray spectroscopy (EDS) images of the PVA/Br-IL film, in Fig. 2A(V)–(IX), show that the Br element is well dispersed both on the surface and inside the film, which also means that most $[HMIM]^+Br^-$ molecules form stable hydrogen bonds with water and PVA polymer backbones.

For polymer network characterization, as shown in Fig. 2C, the characteristic bands for $[HMIM]^+Br^-$ were observed at 1166 cm^{-1} (C–N stretching) and 622–756 cm^{-1} (NH$_2$ & N–H wagging). These characteristic peaks can also be observed in the PVA/Br-IL film. All these peaks show that $[HMIM]^+Br^-$ has been sufficiently dispersed in the film. The broad peak between 3000 and 3600 cm^{-1} refers to the O–H bonds, which are provided by PVA and sufficiently bound water.[26] Compared with pure PVA, there are two more small peaks observed from the curve of the PVA/Br-IL film, which indicates that $[HMIM]^+Br^-$ provides more hydrogen-bonding points for the whole system to trap more bound water. Benefiting from the larger amount of bound water, it will be more effective in enhancing free-charged ions migrating between and across polymer chains under an electric field. In summary, the introduction of Br-IL can soften the polymer network and induce the direction of crystallization, which will improve the spatial orientation. Meanwhile, the better orientation of the polymer/Br-IL network will have a significant effect on the increase in conductivity. Moreover, the penetration of Br-IL into the PVA network can improve the anisotropic mechanical properties of the PVA film and anisotropic mechanical properties, such as flexibility. For convenience, unless otherwise specified, the ion-conductive PVA film with a content of 100 wt% $[HMIM]^+Br^-$ was used for all tests.

Fig. 1 The schematic diagram of the experimental study of the PVA/Br-IL ion-conductive film.

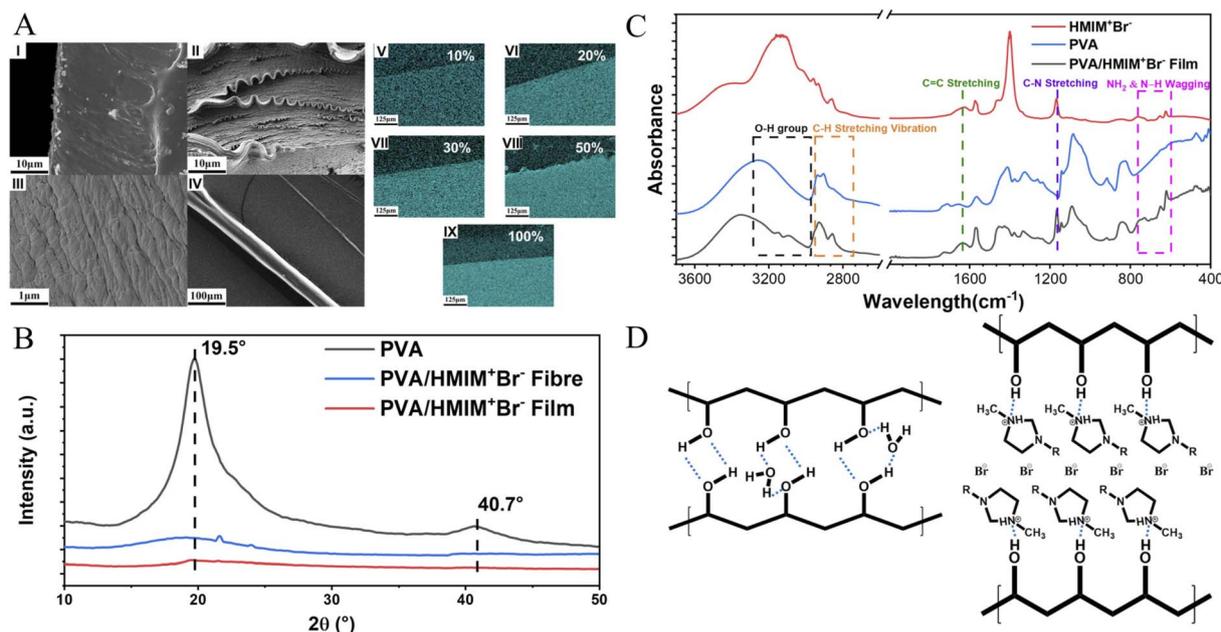© 2023 The Author(s). Published by the Royal Society of Chemistry

Fig. 2 (A) SEM images of the cross-section area of (I) PVA film, (II and III) PVA/Br-IL film with 10 μm (II) and 1 μm (III) scale bar, and (IV) PVA/Br-IL fibre, and (V–IX) EDX images of PVA/Br-IL film with different concentrations of $[HMIM]^+Br^-$, with bromide in green. (B) X-ray diffraction patterns of PVA and PVA/Br-IL fibre and film. (C) FTIR spectra of $[HMIM]^+Br^-$, PVA and the PVA/Br-IL film. (D) Schematic illustration of possible intermolecular interactions involved in PVA/Br-IL film formation.

2.2 Mechanical properties of the PVA/Br-IL film

2.2.1 Tensile behaviour of the film. To investigate the effect of Br-IL in a polymer network, the typical tensile tests were done, and it is found that PVA films exhibit strong plastic behaviour (Fig. 3A). The strong plastic properties allow the PVA film to maintain structural integrity and continuity under abnormal external stresses. However, the films may be disintegrated due to repeated shape variation. Compared with PVA
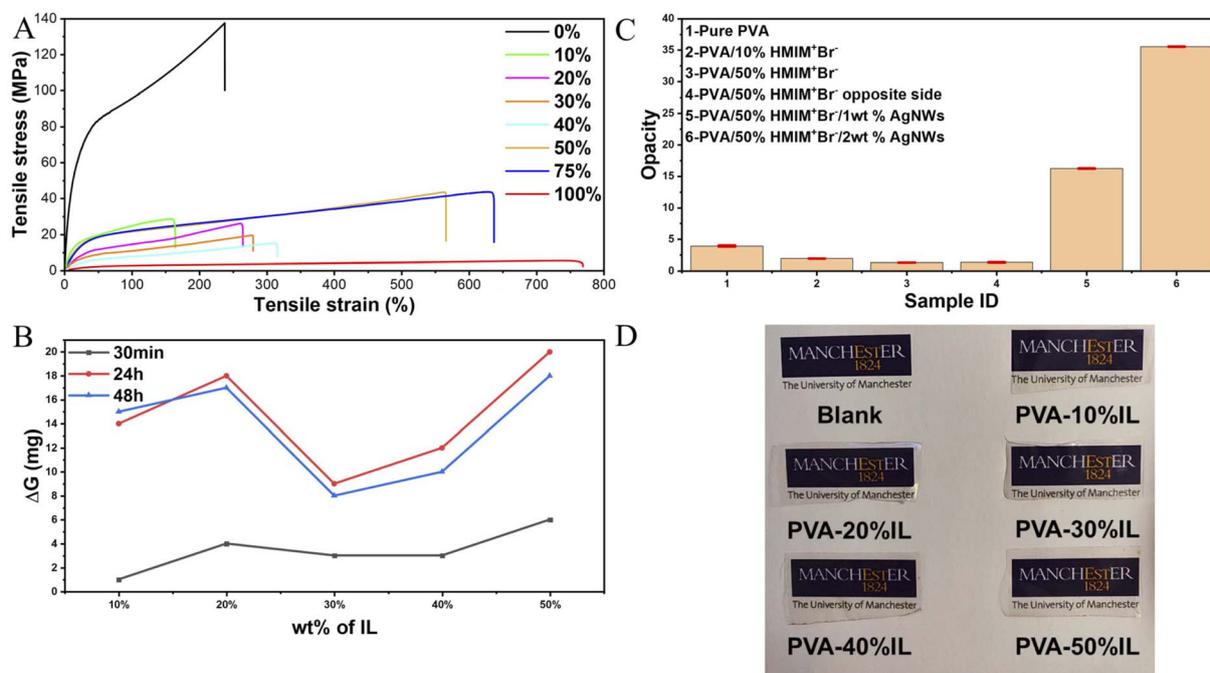

Fig. 3 (A) Tensile stress–strain curves, (B) moisture regain, (C) opacity, and (D) photographs of PVA films with different concentrations of $[HMIM]^+Br^-$.

films, Br-IL modified films show better elastic properties. It can be clearly found that there is a significant drop in Young's modulus of Br-IL modified films, which is even lower than one-quarter compared with PVA films. This is mainly due to the introduction of Br-IL reducing the crystallinity and improving the anisotropic properties. And as a result, benefiting from the lower modulus, the flexibility of Br-IL modified films is significantly enhanced and more suitable for wearable sensor applications. Moreover, although the tensile strength of different concentrations of Br-IL modified films at the breaking point is lower than that of pure PVA film, these PVA/Br-IL films exhibit much better ductility, which is up to nearly 600%.

The main reason for such a noticeable improvement between the pure PVA and modified films is that the function of the ionic liquid is similar to that of lubricating oil between polymer chains. It allows the polymer chains to have more displacement relative to adjacent chains, and as a result, the film will have a higher elongation ratio at the macro level. Besides, the hydrogen bonds between PVA chains are the main connection and will absorb energy during deformation. With the addition of ionic liquid, more hydrogen bonds can be formed not only between PVA chains but also between PVA and ionic liquids. Benefiting from the internal connection in the ionic liquid, which is an ionic bond, the double-bonded system containing hydrogen bonds and ionic bonds can have a much better buffer effect compared with the unitary hydrogen bond system.

2.2.2 Moisture regain behaviour of the PVA/Br-IL film. Aiming to figure out the amount of free water and moisture absorption rate of the PVA/Br-IL network, conventional moisture regain was tested on films with different amounts of IL. As shown in Fig. 3B, when the IL was present in a relatively low content ratio in the whole system, the PVA polymer network played an important role in moisture regain. Large quantities of OH groups on the polymer chain can absorb massive amounts of water from the air into the polymer network. With the increasing content of IL, the gaps and pores in the polymer network were filled by IL and hydrogen bonding has already been formed between PVA and IL, which means both have a decreasing water absorption ability. It's clear that from 30% to 40%, the films have poor moisture regain ability. However, from 40% to 50%, the ionic liquid takes the place of PVA to become the main part for absorbing water. As determined before, the ionic liquid used in this system has good solubility in an aqueous solution. So, while the system has a high content of IL, the whole film can absorb even more water than the PVA network. Benefiting from the strong moisture regain ability of Br-IL, along with its significant hydrogen-bonding towards bound water, the whole system is endowed with a good humidity sensing behaviour while the large amount of bound water will guarantee the ion channels.

2.2.3 Opacity of the film

As a homogeneous film, compared with wearable devices based on carbon or metal solid materials, high transparency will further give the PVA/Br-IL film great potential for use in a variety

of sensing scenarios, especially when taking aesthetics into consideration. From Fig. 3C, it is clear that the pure PVA film has a relatively good opacity behaviour, with nearly 96% transparency. However, it is still dwarfed by the transparency of the PVA/Br-IL film, which is 98% for the PVA/10% [HMIM]$^+$Br$^-$ film and 98.7% for the PVA/50% [HMIM]$^+$Br$^-$ film. It is already known that the opacity of a solid polymer is related to the degree of crystallinity of the polymer system. As reported, a DMSO/water binary solvent system could dramatically increase the transparency of pure PVA hydrogel.[27,28] A similar phenomenon is also observed between PVA and [HMIM]$^+$Br$^-$. From the XRD figure, it is found that the ionic liquid can significantly reduce the degree of crystallinity of PVA. Combined with the unidirectionally aligned micro-fibrous morphologies from the SEM image, it is concluded that the ionic liquid played a similar role to DMSO towards the PVA crystallinity zone. The dissolution of [HMIM]$^+$Br$^-$ in water will form a 3D network structure which will impose a restriction on the crystallization of PVA molecules in 3D while promoting it in 2D. Such a series of influences on the crystallisation process of PVA will result in the crystallization zones of the final film being at a lower level of volume but highly directional.

2.3 Multi-sensing performance of the PVA/Br-IL film

The multiple stimuli responsive characteristics of this IL-based PVA flexible film sensor (about 70 μm thick) were evaluated by measuring its electrical current under fixed 1 V voltage under different conditions at room temperature. The sensitivity of the sensor was determined using the following equations.

$$R = \frac{1}{I}$$

$$\text{Sensitivity} = \frac{\Delta R}{R_0} \times 100\% = \frac{R - R_0}{R_0} \times 100\%$$

where R and R_0 are the resistance under the given and initial test conditions, respectively (the test method is described in detail in the Experimental section).

2.3.1 Strain-sensing behaviour. The PVA/Br-IL tensile strain film sensor exhibits excellent performance in detecting large strains of human finger joints. The real-time dynamic response curve in Fig. 4A indicates that the sensor can recognize the bending of finger joints and elbows at 45° and 90°. Meanwhile, the sensor works for 15 cycles of loading–unloading, and the strain sensor shows similar behaviour for each bending–releasing cycle, that is, once the bent finger is relaxed, the film recovers to the initial state and the resistance also returns to the unstretched state. The similar repeatable curve indicates that the sensor's signal is stable and repeatable. Besides, considering the variability and complexity of real environments, response tests were also carried out at different temperatures. Fig. S8† shows the same response curves under finger bending–relaxing cycles with different bending speeds, which also exhibits good repeatability. As illustrated in Fig. 4A and S7,† such kind of film sensor could distinguish large-scale motions
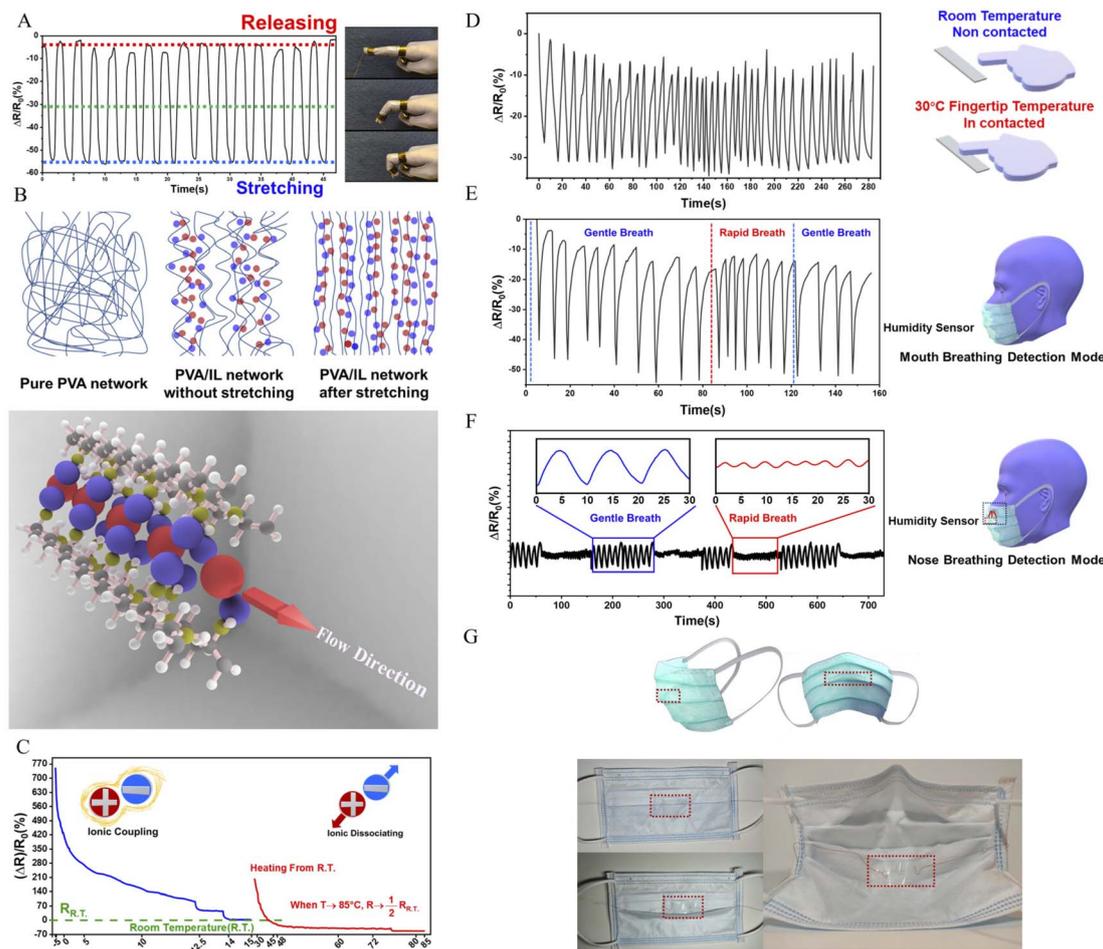
Fig. 4 (A) Relative resistance changes of the PVA/Br-IL film during stretching, (B) schematic illustration of possible variations of the polymer network during stretching and the ion-conducting mechanism. (C and D) Relative resistance changes of the PVA/Br-IL film (C) under continuous temperature variation, and (D) under continuous short-term stimulations. (E–G) Relative resistance changes of the PVA/Br-IL film for (E) the mouth breathing mode and (F) nose breathing mode, and (G) photograph illustrations of the sensor attached to a face mask.

and gentle movements of the human body, including the bending of joints and swallowing action.

What's more, it is worth noting that the resistance had a sharp drop at the instance when the finger started to bend instead of an increased resistance which is unlike what is observed for other common conductive materials, such as silver, copper and carbon, that is, the PVA/Br-IL film shows an unprecedented strain-induced ionic conductivity boost. Such a surprisingly opposite trend of strain-conductivity is similar to the work reported by Yao *et al.* It is concluded that IL will mainly solvate the soft spacers of the PVA region *via* selective cation adsorption, while rigid mesogens would force the anions to move only between them which contributes to ionic conductivity. Before stretching, the fibre network shows a nematic mesophase state with a slightly aligned polydomain. In this state, ions are dispersed and restricted in the network, which leads to a low ion transport behaviour. When the film is gradually stretched, an apparent nematic-to-smectic phase transition will happen between the polymer and ionic liquid and the ion-conducting performance will be boosted, thereby achieving

ultra-fast ion transport performance which is similar to the role of "swimming lanes", which is illustrated in Fig. 4B.

2.3.2 Temperature-sensing behaviour. In order to determine the thermal sensitivity of the PVA/Br-IL film, the electrical conductivity variation between −5 °C and 85 °C was detected. The temperature sensing mechanism was developed based on the unique electrochemical characteristics, and temperature-dependent ion dissociation of the ionic liquid.[29] As schematically shown in Fig. 4C and D, the electrical characteristics of the PVA/Br-IL temperature film sensor were investigated by measuring resistance variation in the temperature range from 0 °C to 85 °C. The responsivities of conductivity over temperature are defined by the same equation used for the strain-sensing test. The ratio $\frac{\Delta R}{R_0}$ was found to decrease by nearly 8 times from 0 °C to room temperature. Meanwhile, it was also found that upon heating the sensor up to 85 °C, the resistance of the PVA/Br-IL temperature film sensor dropped slightly to under half that at room temperature. The same downward trend of resistance with temperature over the two periods of heating might be due to the

dissociation of the ions. When freezing the film down to 0 °C, the crystallization zone in the interior of the polymer network will be more rigid and hinder the movement of ions. Also, anions and cations of the ionic liquid tend to form more coupling connections at lower temperature and this will hinder the accumulation of the ions at the interface between the film and electrodes. During the heating process, the stiff polymer network will be gradually softened and coupled ions will dissociate to become free anions and cations which can be driven under an applied electrical field. Moreover, the emergence of a substantial increase in resistance at the beginning of heating can be found in Fig. 4C. It might be concluded that the sudden temperature rise will dissociate a huge amount of free ions and this will result in a chaotic status that will also decrease the performance of directional movement of anions and cations.

Based on the unique thermal sensitivity behaviour of Br-IL, the film sensor could detect short-term temperature stimulations, even if this stimulus comes from the fingertip (Fig. 4D and S12†). Here, each time interval represents a complete contact cycle between the fingertip and the film sensor. A clear resistance change, in the range of 20–30%, could be found for each contact cycle. Also, like the strain sensor behaviour tests, the temperature-sensing behaviour was also tested in different environments (Fig. S9 and S10†). As illustrated in Fig. S9,† the same resistance change curves could be found when samples were at −2.5 °C and room temperature. However, completely opposite changes were observed in the $\frac{\Delta R}{R_0}$ curves at 45 °C and that is due to the relatively low temperature of the fingertips which will contribute to the cooling of the contact area between the film and the fingertip, and that will further increase the resistance of the film. What's more, in Fig. S10,† the stable resistance change curves are the same as those in Fig. S9,† which indicates that such film sensors have a reliable thermal sensing performance in different environments.

2.3.3 Humidity-sensing behaviour. Given that most commercial wearable sensor applications necessitate measurement of relative humidity (R.H.) in areas of limited airflow, it was important to assess the reliability of the PVA/Br-IL sensor film in still air. In Fig. 4E and F, the real-time dynamic sensing responses to both gentle and rapid air flow under mouth and nose breathing styles are recorded. They indicate that, with the air flowing out of the human body, the resistance decreased dramatically as the R.H. increased. Such a changing trend in the conductivity of the film is related to the rise of moisture in a small, confined environment and condensation on the surface of the film. For the two types of breathing modes, under the mouth and nose, the dynamic R sensitivity curve shows that the IL-based sensor has a quick responsive behaviour (about 0.5 s) towards human breathing and the changing trend closely matches the breathing speed. Moreover, like the two previous sensing behaviour tests, breathing tests were also carried out at different temperatures (Fig. S11†). Considering the common ambient temperature and rare extremely high and low temperatures humans might face in summer and winter, four temperature points, −5 °C, 30 °C, 40 °C, and 50 °C, were selected for tests. Under those four different situations, stable

relative resistance change curves show the same trend and quick response time as tests at room temperature. We can therefore draw the conclusion that the polymer/IL dual-network serves as a highly ion-conductive pathway that enables rapid migration of ions along with a fast response time.

The basic humidity-sensing response mechanism of the IL-based PVA sensor can be explained as follows. A series of models all consider the partition of water in polymer network uptake into two different ways which are commonly called bonded and unbound. Initially, when breathing out, a moisture-rich air flow filled the space between the medical mask and face. Once the IL-based PVA sensor has contact with the moisture, the chemical absorption of water will occur first. During this absorption process, the alcoholic hydroxyl group (Xn–OH) in the PVA molecular chain will change into the active state. The water molecule will establish hydrogen bonding with the hydrophilic sites on the PVA polymer. However, due to the introduction of the ionic liquid, a kind of strong amphoteric addition will result, with the PVA/Br-IL dual network already almost reaching its maximum dynamic balance of chemical absorption of water. Numerous hydrogen bonds have already formed and been stabilized among PVA, HMIM Br and water. Under this circumstance, the mechanism of moisture absorption will directly jump to the physical absorption and formation of unbound water. The physical absorption of water will continue by the corresponding water molecules attached to free hydroxyl groups in the deep narrow hollow space that still exists. Higher humidity levels give rise to a higher number of physically adsorbed layers formed in the shallow level of the whole system, which will still continuously lower the resistance of the film. And in the desorption process, along with the unbound water at a shallow level transported out of the PVA/Br-IL film, part of the unbound water at a deep level is still trapped and covered by the giant ionic liquid molecule which has undergone displacement. At this time, higher humidity levels mean more physically absorbed water layers formed and the removal of these layers is much slower. That may be the reason that, when breathing by mouth, the changing slope of desorption was rather lower than that of adsorption, which means the recovery time of the IL-based sensor is rather slower than the response time. Meanwhile for nose breathing, the recovery time of the sensor is almost the same as the response time. What's more, it is found that good moisture regain ability is like a "double-edged sword". The PVA/Br-IL film is endowed with good humidity-sensing performance. However, the noticeable drift in the resistance–humidity curve can be attributed to the fact that during long-time cyclic breathing, part of the moisture was firmly captured by the film and could no longer vapourize from the system, which is gradually affecting the resistance during the test. Although there is a certain resistance deviation, the resistance curve is always similar, indicating that our hydrogel sensor has high durability in practical applications.

2.4 Reusability and recyclability of the PVA/Br-IL film sensor

The multi-functional sensor we prepared fully consists of the integration of stable ionic liquid-based nanofluids. As

environmentally friendly and recyclable materials, PVA films show good shape stability with almost invariable physical properties under ambient conditions, which ensures their excellent sensing functions in daily applications. Benefiting from its outstanding sensing stability under different working conditions, even if the film sensor is contaminated by dust on the surface, it's convenient to reuse *via* a simple dust clean-up, self-balancing in an air-conditioned room and re-assembling into a functional device for further use. If irreversible invasive damage happens to the sensor, a simple dissolving–filtering method could be used to get rid of any other insoluble materials for the formation of the next film, as shown in Fig. S13.† What's more, it has already been proved that the introduction of ionic liquids does not affect the original dissolution characteristics of PVA. Fig. S14† illustrates one cycle of the PVA/Br-IL film dissolving process. 15 seconds after the film was immersed in hot water (90 °C), the edge shapes of the film disappeared, which means the integration of ionic liquid will not affect the dissolvability of PVA at an elevated temperature. 90 seconds later, the entire PVA/Br-IL film was dissolved into water to form a transparent and homogeneous solution. The concentrated solution under continuous heating in the recycle bath can be used for the fabrication of new film sensors with different sizes and shapes.

Mechanical tests also show that there is no obvious mechanical tensile property deterioration after several cycles, as shown in Fig. 5A. The good sensing and mechanical retainability of the PVA/Br-IL films ensure the recycling usage ability. What's more, benefiting from all water-soluble chemicals, as the number of cycles increases, the attrition rate still remains within a manageable range (Fig. 5B). Therefore, compared with conventional sensors based on non-degradable materials like metals, silicon and other traditional solid polymers, the PVA/Br-IL film sensor has the advantage of reusability and recyclability. In addition, different from previously reported recyclable sensors which require not only extreme conditions like strong acid or alkali conditions but also long-time operation for improving the recycling ratio, the PVA/Br-IL based sensor can be fully dissolved in hot water within several minutes, which is convenient, rapid and energy saving for the recycling process.

3 Experimental section

3.1 Materials

Poly(vinyl alcohol) (PVA) (alcoholysis degree: ≥99%, M_n: 146 000–186 000), 1-methylimidazole (≥99%) and 1-bromohexane

(98%) were purchased from Alfa Aesar. Silver nanowires (diam. $\times$ L 120–150 nm $\times$ 20–50 μm, 0.5% (isopropyl alcohol suspension)) were purchased from Sigma-Aldrich. Poly(vinyl alcohol) and silver nanowires were used without further purification, and deionized water was used for all experiments.

3.2 Synthesis of $[HMIM]^+Br^-$

Firstly, both 1-bromohexane and 1-methylimidazole were purified *via* decompression distillation. Then after purification, 1-methylimidazole was pre-vortexed for 5 min along with heating to 140 °C and 1-bromohexane was added to the constant pressure dropping funnel. For the next step, 1-bromohexane was introduced to 1-methylimidazole one drop at a time. The whole reaction was carried out under a nitrogen atmosphere with vigorous stirring for 12–24 h. After the reaction, the product was washed with petroleum ether to remove the remaining reactants.

3.3 Fabrication of the PVA film and $[HMIM]^+Br^-$ modified PVA film/fibre

The 4 wt% polyvinyl alcohol film was prepared by dissolving PVA into 85 °C deionized water, then transferring it into a model and drying it under a vacuum state after degassing. The $[HMIM]^+Br^-$ modified PVA film was prepared by adding $[HMIM]^+Br^-$ into 4 wt% PVA aqueous solution followed by the same methods as previously used on PVA films. Different weight ratios, from 0% to 100%, of $[HMIM]^+Br^-$ over PVA were prepared for further research on how IL will affect the mechanical properties of polymer films. The $[HMIM]^+Br^-$ modified PVA fibre was prepared by concentrating PVA and $[HMIM]^+Br^-$ mixed solution. When the majority of water was left in the mixture, it could be shaped and stretched to form a fibre.

3.4 Instruments and characterization methods

Fourier transform infrared spectroscopy (FTIR) was employed to probe the functional groups and the intermolecular hydrogen bonds between the Br-IL and the PVA chains. FTIR characterization was carried out on a Nicolet 5700 FT-IR spectrophotometer. The spectra were recorded within the range of 400–4000 cm^{-1}.

The morphological structure of the PVA and PVA/Br-IL films/fibres was observed by scanning electron microscopy (SEM),
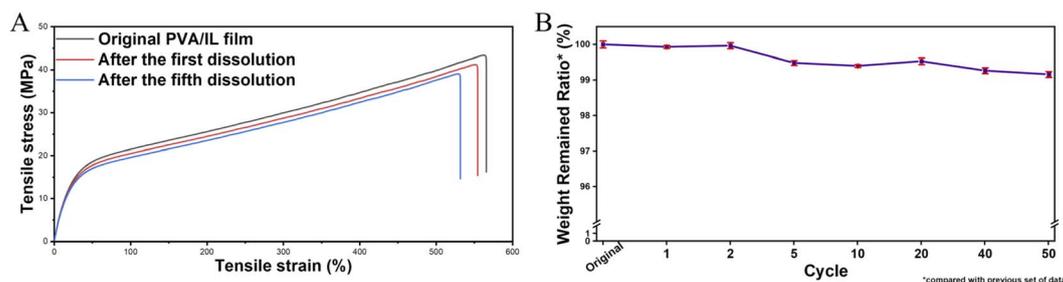

Fig. 5 (A) Tensile stress−strain curves of the primary PVA/Br-IL film and recycled film, and (B) recycling attrition rate of the PVA/Br-IL film.

using a Zeiss Ultra 55 FEG-SEM operated at a 1.5 kV/3 kV acceleration voltage, which depends on different samples. Energy-dispersive X-ray spectroscopy (EDX) was also performed at a 15.0 kV acceleration voltage. To prepare the sample, cut PVA and PVA/Br-IL films were fixed on a metal stub with carbon tape and were then coated with 5 nm of gold/palladium alloy using a Quorum Au/Pd coater.

High-resolution powder X-ray diffraction (XRD) was applied to reveal the crystalline and amorphous structures of the PVA and PVA/Br-IL films/fibres and the measurements were conducted at room temperature on a PANalytical X'Pert Pro (model XRD5) versatile machine.

Thermogravimetric analysis (TGA) was carried out from 30 to 750 °C under a nitrogen atmosphere (90.0 mL min^{-1}) using a TGA Q500 thermogravimetric analyzer. Samples (5–10 mg) were analyzed in a platinum pan with 10 °C min^{-1} being the heating rate.

An Instron 5564 tensile test machine equipped with a 100 N load cell was used to test all the mechanical properties in the conditional room. The stress/strain measurements were carried out with film samples which were cut into a dumbbell shape at an elongation speed of 30 mm cm^{-1}. The tensile strain was calculated by dividing the distance between clamps by the original length of the samples, and the tensile stress was measured by dividing the applied force by the cross-sectional area. Young's modulus was estimated from the initial slope of the stress/strain curve.

An Elrepho 450X spectrophotometer was used to test the optical properties in the conditional room. The colour, brightness, opacity, diffuse reflectance factors, yellowness, and whiteness of the prepared samples were tested at 10 nm intervals in the 400–700 nm visible spectrum.

An IviumStat.h electrochemical workstation from Ivium Technologies B.V. was used to test the electrochemical properties of the prepared samples. An MFIA 500 kHz impedance analyzer from Zurich Instruments along with the IviumStat.h was used to evaluate the multi-sensing performance of the PVA/Br-IL film. Samples were cut 1 cm wide by 5 cm in length. Copper tape and wires were used to connect samples to the instruments. All tests were carried out in the conditioning room unless otherwise specified. Normal surgical masks were used to simulate the breath under a medical face mask.

The films prepared for moisture regain measurement were dried to constant weight at 60 °C in a vacuum oven. Films before and after drying were accurately weighed and recorded as W_0 and W_1. All the tests were repeated more than three times and the moisture regain value was calculated using:

$$\text{Moisture regain value} = \frac{W_0 - W_1}{W_0}$$

4 Conclusions

In this work, to solve the problems of non-recyclability and environmental pollution of traditional wearable devices, we designed a new type of soft wearable device, whose recyclability

has already been proved and theoretically this device can be recycled and reused an unlimited number of times. Benefiting from the introduction of [HMIM]$^+$Br$^-$, the flexibility and stretchability of the PVA film are enhanced, which indicates that the addition of [HMIM]$^+$Br$^-$ could not only enhance the mechanical behaviours in the wearable sensor area but also make the whole system 100% recyclable. Moreover, the addition of [HMIM]$^+$Br$^-$ does not change the overall homogeneous phase properties, which means the designed device is endowed with good fatigue resistance. Additionally, the ionic conductivity of the PVA/Br-IL network could be explained by a phenomenon known as the swimming lane effect. This particular polymer ion channel effect endows PVA with unique ionic conductivity and the PVA/Br-IL films also show responsive behaviours towards elongation, humidity and temperature, making it an ideal material for fabricating multi-functional sensors. Thus, the PVA/Br-IL films promise fully recyclable and wearable sensors. In addition, they offer a viable material strategy for the future green manufacturing and sustainable development of wearable technology.

Conflicts of interest

There are no conflicts to declare.

Acknowledgements

Notes and references

1 H. Ma, F. Lv, L. Shen, K. Yang, Y. Jiang, J. Ma, X. Geng, T. Sun, Y. Pan, Z. Xie, M. Xue and N. Zhu, *Energy Environ. Mater.*, 2022, **5**, 986–995.
2 R. Ma, Z. Xu and X. Wang, *Energy Environ. Mater.*, 2022, e12464.
3 D.-M. Drotlef, M. Amjadi, M. Yunusa and M. Sitti, *Adv. Mater.*, 2017, **29**, 1701353.
4 A. Koh, D. Kang, Y. Xue, S. Lee, R. M. Pielak, J. Kim, T. Hwang, S. Min, A. Banks, P. Bastien, *et al.*, *Sci. Transl. Med.*, 2016, **8**, 366ra165.
5 W. Gao, S. Emaminejad, H. Y. Y. Nyein, S. Challa, K. Chen, A. Peck, H. M. Fahad, H. Ota, H. Shiraki, D. Kiriya, *et al.*, *Nature*, 2016, **529**, 509–514.
6 H. Liu, Q. Li, S. Zhang, R. Yin, X. Liu, Y. He, K. Dai, C. Shan, J. Guo, C. Liu, C. Shen, X. Wang, N. Wang, Z. Wang, R. Wei and Z. Guo, *J. Mater. Chem. C*, 2018, **6**, 12121–12141.
7 S. Yao and Y. Zhu, *Nanoscale*, 2014, **6**, 2345–2352.
8 S. Ding, J. Jiu, Y. Gao, Y. Tian, T. Araki, T. Sugahara, S. Nagao, M. Nogi, H. Koga, K. Suganuma and H. Uchida, *ACS Appl. Mater. Interfaces*, 2016, **8**, 6190–6199.
9 J. Di, X. Zhang, Z. Yong, Y. Zhang, D. Li, R. Li, Q. Li, J. Di, X. Zhang, Z. Yong, Y. Zhang, D. Li, R. Li and Q. Li, *Adv. Mater.*, 2016, **28**, 10529–10538.

10 L. Q. Tao, K. N. Zhang, H. Tian, Y. Liu, D. Y. Wang, Y. Q. Chen, Y. Yang and T. L. Ren, *ACS Nano*, 2017, **11**, 8790–8795.

11 J. Shintake, Y. Piskarev, H. Jeong, D. Floreano, J. Shintake, S. H. Jeong, D. Floreano and Y. Piskarev, *Adv. Mater. Technol.*, 2018, **3**, 1700284.

12 K. Du, E. H. Ang, X. Wu and Y. Liu, *Energy Environ. Mater.*, 2022, **5**, 1012–1036.

13 X. Tao, S. Liao and Y. Wang, *EcoMat*, 2021, **3**, e12083.

14 B. Wan, M.-S. Zheng, X. Yang, X. Dong, Y. Li, Y.-W. Mai, G. Chen and J.-W. Zha, *Energy Environ. Mater.*, 2023, e12427.

15 N. Mittal, A. Ojanguren, M. Niederberger and E. Lizundia, *Adv. Sci.*, 2021, **8**, 2004814.

16 Y. Gao, Y. Zhang, X. Wang, K. Sim, J. Liu, J. Chen, X. Feng, H. Xu and C. Yu, *Sci. Adv.*, 2017, **3**, e1701222.

17 X. Liu, J. Miao, Q. Fan, W. Zhang, X. Zuo, M. Tian, S. Zhu, X. Zhang and L. Qu, *Adv. Fiber Mater.*, 2022, **4**, 361–389.

18 H. Nguyen, R. de Vries and S. Stoyanov, *Green Chem.*, 2022, **24**(9), 3824–3844.

19 J. Gao, J. Wang, Q. Xu, S. Wu and Y. Chen, *Green Chem.*, 2021, **23**(15), 5633–5646.

20 M. Tavakolizadeh, A. Pourjavadi, M. Ansari, H. Tebyanian, S. Seyyed Tabaei, M. Atarod, N. Rabiee, M. Bagherzadeh and R. Varma, *Green Chem.*, 2021, **23**(3), 1312–1329.

21 L. Sun, H. Huang, Q. Ding, Y. Guo, W. Sun, Z. Wu, M. Qin, Q. Guan and Z. You, *Adv. Fiber Mater.*, 2022, **4**, 98–107.

22 D. Ma, D. Yuan, C. Ponce de León, Z. Jiang, X. Xia and J. Pan, *Energy Environ. Mater.*, 2022, DOI: **10.1002/eem2.12301**.

23 J. Zheng, W. Li, X. Liu, J. Zhang, X. Feng and W. Chen, *Energy Environ. Mater.*, 2023, DOI: **10.1002/eem2.12422**.

24 L. C. Fernandes, D. M. Correia, N. Pereira, C. R. Tubio and S. Lanceros-Méndez, *ACS Appl. Polym. Mater.*, 2019, **1**, 2723–2730.

25 D. M. Correia, L. C. Fernandes, P. M. Martins, C. García-Astrain, C. M. Costa, J. Reguera and S. Lanceros-Méndez, *Adv. Funct. Mater.*, 2020, **30**, 1909736.

26 L. Fan, L. Hu, J. Xie, Z. He, Y. Zheng, D. Wei, D. Yao and F. Su, *Biomater. Sci.*, 2021, **9**, 5884–5896.

27 Y. Hou, C. Chen, K. Liu, Y. Tu, L. Zhang and Y. Li, *RSC Adv.*, 2015, **5**, 24023–24030.

28 S. Wu, Y. Alsaid, B. Yao, Y. Yan, Y. Zhao, M. Hua, D. Wu, X. Zhu and X. He, *EcoMat*, 2021, **3**, e12085.

29 M. A. Gebbie, H. A. Dobbs, M. Valtiner and J. N. Israelachvili, *Proc. Natl. Acad. Sci. U. S. A.*, 2015, **112**, 7432–7437.